Efficient Permanent Magnet Temperature Modeling and Estimation for Dual Three-Phase PMSM Considering Inverter Nonlinearity

Guodong Feng, *Member, IEEE*, Chunyan Lai, *Senior Member, IEEE*, Wenlong Li, *Senior Member, IEEE*, Ze Li, *Student Member, IEEE*, and Narayan C. Kar, *Senior Member, IEEE*

***Abstract*—Accurate temperature information is crucial to dual three-phase permanent magnet synchronous machine (DT-PMSM) drives. Therefore, this article proposes two efficient models for permanent magnet temperature estimation of DT-PMSMs. The proposed models are derived through current injection in the reference frame that does not contribute to torque production. Through current injection, the proposed models can fully explore the two sets of machine equations to cancel winding resistance and machine inductances. To improve the estimation performance, inverter nonlinearity is compensated in the first model and cancelled in the second model. In comparison to existing methods, the proposed approach is computationally efficient and robust to parameter variation, magnetic saturation, and inverter nonlinearity. Moreover, the current injection will not affect the machine torque production and control performance. The proposed estimation approach is evaluated on a laboratory DT-PMSM under various operating conditions.**

***Index Terms*—Current injection, dual three-phase permanent magnet synchronous machines (DT-PMSM), inverter nonlinearity, permanent magnet temperature (PMT) estimation.**

I. Introduction

DUAL three-phase permanent magnet synchronous machines (DT-PMSMs) have stimulated extensive research attentions in both industrial and commercial applications due to their high torque density, reduced per phase power rating, and fault tolerant capability in comparison to existing three-phase PMSMs [1]–[5]. For instance, the DT-PMSM, consisting of two sets of three-phase windings, can operate with one or two phases under fault, while the three-phase PMSM is unable to operate with one phase opened without hardware modification [6]–[9]. For DT-PMSMs, accurate parameters are critical to high-performance, efficient and reliable control. Among various parameters, permanent magnet temperature (PMT) is especially important as the torque performance of DT-PMSM decreases with the increase of PMT [10]–[12]. Moreover, accurate PMT can be utilized to monitor the condition of permanent magnets (PMs) to avoid permanent demagnetization of the PMs and motor failure. Therefore, this article investigates PMT estimation of DT-PMSMs and proposes efficient estimation approaches.

For three-phase PMSMs, PMT can be obtained through mainly three strategies. The first one is the direct measurement of PMT. For instance, Hall sensors are investigated for PMT estimation in [13]. However, PMs in the rotor will rotate during machine operation, which imposes challenges to the measurement especially at high-speed conditions. Moreover, installation of noncontact temperature sensors will add additional cost concern and other practical challenges. The second strategy is based on the thermal model, in which the thermal networks are employed to model the heat flow in the motor for temperature estimation [14]–[16]. This approach is capable of estimating the temperature of any parts of the motor which, however, requires accurate losses information and/or geometric structure data. The third strategy is based on the machine model consisting of PMT dependent parameters. For instance, PM flux linkage decreases linearly as PMT increases in the linear operation region [17]. Therefore, PMT can be estimated from the PM flux linkage with the use of available measurements. In comparison to first and second strategies, the third one has stimulated considerable research interests especially for conventional three-phase PMSMs due to cost effectiveness, efficiency, and robustness. Hence, this article focuses on the third strategy exploring the temperature-dependent parameters for PMT estimation of DT-PMSMs.

There is limited literature on DT-PMSM PMT estimation. However, most of existing approaches for three-phase PMSM can be extended to the DT-PMSMs, in which the PMT is estimated from temperature-dependent machine parameters. The existing approaches can be divided into the model-based approach and signal injection-based approach. In the model-based approach [18]–[22], the estimation model is first derived from machine dq-axis equations and then estimation algorithms such as least squares are applied to estimate the PM flux linkage for PMT estimation, which can estimate PMT from the available measurements. However, accurate machine inductances and/or resistance are required, but parameter variation is inevitable during machine operation due to temperature rise and magnetic

Manuscript received June 19, 2019; revised September 16, 2019 and October 31, 2019; accepted November 22, 2019. Date of publication November 25, 2019; date of current version March 13, 2020. Recommended for publication by Associate Editor L. Chang. *(Corresponding author: Guodong Feng.)*

G. Feng is with the School of Intelligent Systems Engineering, Sun Yat-sen University, Guangzhou 510275, China (e-mail: qqfengguodong@gmail.com).

C. Lai is with the Department of Electrical and Computer Engineering, Concordia University, Montreal, QC H3G 1M8, Canada (e-mail: chunyan.lai@concordia.ca).

W. Li, Z. Li, and N. C. Kar are with the Department of Electrical and Computer Engineering, University of Windsor, Windsor, ON N9B 3P4, Canada (e-mail: wenlong.li@uwindsor.ca; li111169@uwindsor.ca; nkar@uwindsor.ca).

Color versions of one or more of the figures in this article are available online at http://ieeexplore.ieee.org.

Digital Object Identifier 10.1109/TPEL.2019.2956353

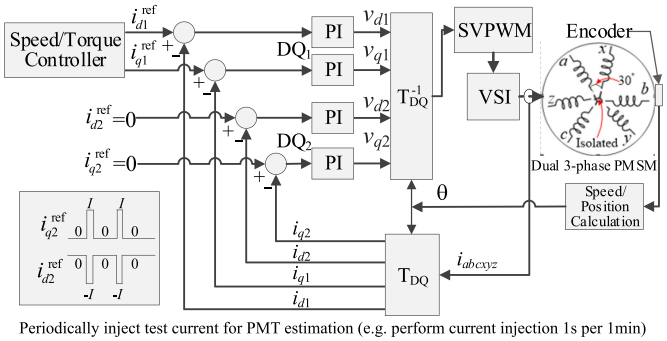

Fig. 1. DT-PMSM control with current injection in non-torque-contributing DQ_2 reference frame for PMT estimation.

saturation. Moreover, this approach can be affected by the inverter distortion. In the signal injection-based approach, high frequency (HF) signal is injected into the motor to estimate the PMT from the signal response and HF model [23], [24]. This approach can eliminate the need of machine inductances in PMT estimation, but it still requires accurate winding resistance and temperature.

On the other hand, different from three-phase PMSMs consisting of one set of machine equations, DT-PMSM consists of two sets of equations [25]–[27], which means that there is more flexibility to be explored in the DT-PMSM model for improving the estimation performance. However, direct extending existing approaches to DT-PMSMs is unable to explore this extra flexibility and also requires the machine inductances and/or winding resistance for PMT estimation.

Understanding the limitations of existing approaches and the flexibility of the DT-PMSM model, this article proposes novel PMT estimation approaches for DT-PMSMs that can eliminate the need of machine inductances and winding resistance, which is achieved by current injection in the reference frame that is not contributing to torque production. Specifically, this article derives two estimation models from the DT-PMSM equations. Through current injection, machine inductances and winding resistance are cancelled in the derived models, thus the estimation performance will not be affected by the variation of machine parameters. Since the currents are injected to the frame that has no contribution to torque production, the proposed approach will not affect motor control. Moreover, inverter nonlinearity is modeled, its influence is investigated, and compensation and/or elimination approach is developed for each model. Extensive experiments are conducted to evaluate the proposed approach on an interior DT-PMSM under various operating conditions.

II. Vector Space Decomposition (VSD)-Based DT-PMSM Modeling

The DT-PMSM of interest in Fig. 1 consists of two sets of three phase windings, denoted by (*a*, *b*, *c*, *x*, *y*, *z*), with two isolated neutral points. The phase shift between *a* and *x* is $\pi/6$. In *abcxyz* frame, the DT-PMSM model can be denoted as

$$\begin{cases} u_{abcxyz} = \mathbf{R} i_{abcxyz} + \dot{\lambda}_{abcxyz} \\ \lambda_{abcxyz} = \mathbf{L} i_{abcxyz} + \lambda_{\mathrm{PM},abcxyz} \end{cases} \tag{1}$$

where P_{abcxyz} with $P = u$, i, λ, or λ_{PM} denotes the vector of the phase voltage, current, flux linkage, or PM flux linkage in the *abcxyz* frame, respectively; $\mathbf{L}$ is the inductance matrix; and $\mathbf{R}$ is the resistance matrix.

The VSD model introduces a transformation matrix $\mathbf{T}_{\mathrm{DQ}}$ in (2) to convert (1) into DQ_1 and DQ_2 frames, where $\theta_0 = \theta - \pi/3$ and $\theta_1 = \theta + \pi/3$ with θ being rotor electrical position. The VSD-based steady-state DT-PMSM model can be denoted as follows [27]–[29]:

$$T_{\mathrm{DQ}} = \frac{1}{3}\begin{bmatrix} \cos\theta & -\cos\theta_1 & -\cos\theta_0 & \sin\theta_1 & \sin\theta_0 & -\sin\theta \\ -\sin\theta & \sin\theta_1 & \sin\theta_0 & \cos\theta_1 & \cos\theta_0 & -\cos\theta \\ -\sin\theta & \sin\theta_1 & \sin\theta_0 & -\cos\theta_1 & -\cos\theta_0 & \cos\theta \\ -\cos\theta & \cos\theta_1 & \cos\theta_0 & \sin\theta_1 & \sin\theta_0 & -\sin\theta \end{bmatrix} \tag{2}$$

$$\begin{cases} u_{d1} = R i_{d1} - \omega L_{q1} i_{q1}, \quad u_{q1} = R i_{q1} + \omega \left(L_{d1} i_{d1} + \lambda_0 \right) \\ u_{d2} = R i_{d2} - \omega L_{q2} i_{q2}, \quad u_{q2} = R i_{q2} + \omega L_{d2} i_{d2}. \end{cases} \tag{3}$$

Here, there are two sets of axes denoted by DQ_1 and DQ_2 in (3), $u_{dk}, u_{qk}, i_{dk}, i_{qk}, L_{dk}$, and L_{qk} denote the voltages, currents, and inductances in DQ_k axis, $k = 1, 2$, ω is the rotor electrical speed, and λ_0 is the PM flux linkage. Detailed expressions of the inductances can be found in [27], [31], and they satisfy $L_{d1} < L_{q1}$ for interior DT-PMSM, $L_{d1} = L_{q1}$ for surface-mounted DT-PMSM, and $L_{d2} = L_{q2}$ for both DT-PMSMs.

The DT-PMSM torque equation is [9], [27]

$$t_e = 3P \left(\lambda_0 i_{q1} + \left(L_{d1} - L_{q1} \right) i_{d1} i_{q1} \right) \tag{4}$$

where t_e is the output torque and P is the number of pole pairs. From (4), DQ_2 frame does not contribute to torque production. Fig. 1 presents the VSD model-based DT-PMSM control, in which DQ_1 frame currents are controlled for torque production, while DQ_2 frame currents are set to zero due to no contribution to torque production. The references i_{d1}^{ref} and i_{q1}^{ref} are from outer loop controller, and four PI controllers are employed for current control.

In (3), λ_0 is PMT dependent, thus this article explores the use of (3) for PMT estimation, in which the voltage measurements from four PI current controllers in Fig. 1 will be employed due to the lack of accurate voltage sensors in most industrial drive. However, due to the inverter nonlinearity, the voltages from PI controllers are unequal to the actual voltages supplied to the motor, that is, the inverter will distort the voltages due to reasons such as deadtime. The relationship between the reference and actual voltages can be modeled as

$$\begin{cases} v_{d1} = u_{d1} + D_{d1} V_{\mathrm{dead}}, \quad v_{q1} = u_{q1} + D_{q1} V_{\mathrm{dead}} \\ v_{d2} = u_{d2} + D_{d2} V_{\mathrm{dead}}, \quad v_{q2} = u_{q2} + D_{q2} V_{\mathrm{dead}} \end{cases} \tag{5}$$

where v_{d1}, v_{q1}, v_{d2}, and v_{q2} are the output voltages of the four PI controllers in Fig. 1; $D_{d1}V_{\mathrm{dead}}$, $D_{q1}V_{\mathrm{dead}}$, $D_{d2}V_{\mathrm{dead}}$, and $D_{q2}V_{\mathrm{dead}}$ are inverter distorted terms on v_{d1}, v_{q1}, v_{d2}, and v_{q2}, respectively; V_{dead} is the inverter distorted voltage due to deadtime effect; the expressions and investigations of D_{d1}, D_{q1}, D_{d2}, and D_{q2} are detailed in the Appendix, which will show that they are functions of DQ frame currents and rotor position.

According to [35], the inverter distortion model is applicable to operating conditions with different switching frequencies and speeds. For the given inverter with a fixed deadtime, $V_{\rm dead}$ can be viewed as constant and can be calculated from (55).

Substituting (5) into (3), the DT-PMSM model considering inverter nonlinearity can be denoted as

$$\begin{cases} v_{d1} = Ri_{d1} - \omega L_{q1} i_{q1} + D_{d1} V_{\rm dead} \\ v_{q1} = Ri_{q1} + \omega \left(L_{d1} i_{d1} + \lambda_0 \right) + D_{q1} V_{\rm dead} \\ v_{d2} = Ri_{d2} - \omega L_{q2} i_{q2} + D_{d2} V_{\rm dead} \\ v_{q2} = Ri_{q2} + \omega L_{d2} i_{d2} + D_{q2} V_{\rm dead}. \end{cases} \tag{6}$$

Since D_{d1}, D_{q1}, D_{d2}, and D_{q2} are functions of stator currents and rotor position, it becomes complicated to perform PMT estimation using instantaneous measurements due to the need of rotor position. However, the Appendix shows that the average values of D_{d1}, D_{q1}, D_{d2}, and D_{q2} are independent from rotor position and they are only functions of DQ frame currents and can be calculated from (54). Hence, this article explores the use of the dc values for PMT estimation and use the capital letter to denote the dc value. For instance, V_{d1} denotes the dc value of v_{d1}. A down-sampling factor will be used to achieve a lower sampling rate for PMT estimation, and the arithmetic mean of the data within a predefined period will be used as the dc value. In this way, (6) can be rewritten as (7) by using the dc values, where *V*, *I*, D_D, and D_Q represent the dc values of *v*, *i*, D_d, and D_q, respectively

$$\begin{cases} V_{d1} = RI_{d1} - \omega L_{q1} I_{q1} + D_{D1} V_{\rm dead} \\ V_{q1} = RI_{q1} + \omega \left(L_{d1} I_{d1} + \lambda_0 \right) + D_{Q1} V_{\rm dead} \\ V_{d2} = RI_{d2} - \omega L_{q2} I_{q2} + D_{D2} V_{\rm dead} \\ V_{q2} = RI_{q2} + \omega L_{d2} I_{d2} + D_{Q2} V_{\rm dead}. \end{cases} \tag{7}$$

III. Current Injection-Based PMT Estimation

This section first derives the current injection-based estimation models denoted by M1 and M2, and then proposes methods to compensate and/or cancel the inverter distortion, and finally discusses the Kalman filter-based temperature smoothing and the influence due to model uncertainty.

A. Deriving PMT Estimation Models

To derive model M1, testing currents $-I$ and I will be injected into D_2 and Q_2 frames, that is, setting $I_{d2} = -I$ and $I_{q2} = I$. Current injection in DQ_2 frame will not affect the torque production. As shown in Fig. 1, $(I_{d2},\ I_{q2})$ will be controlled to $(-I, I)$ for a short period and will be controlled back to zero after data collection. The sum of 1st equation in (7) multiplied by I_{d1} and 2nd one in (7) multiplied by I_{q1} is (8), and since I_{d2} and I_{q2} are nonzero, (9) is obtained from 3rd and 4th equations in (7).

$$\begin{aligned} V_{d1} I_{d1} + V_{q1} I_{q1} = {} & RI_{s1}^2 + \omega I_{q1} \left(L_\Delta I_{d1} + \lambda_0 \right) \\ & + \left(I_{d1} D_{D1} + I_{q1} D_{Q1} \right) V_{\rm dead} \end{aligned} \tag{8}$$

$$\begin{aligned} V_{q2} - V_{d2} = {} & R \left(I_{q2} - I_{d2} \right) + \omega \left(L_{d2} I_{d2} + L_{q2} I_{q2} \right) \\ & + \left(D_{Q2} - D_{D2} \right) V_{\rm dead} \end{aligned} \tag{9}$$

where $L_\Delta = L_{d1} - L_{q1}$ and $I_{s1}^2 = I_{d1}^2 + I_{q1}^2$.

Substituting $I_{d2} = -I$, $I_{q2} = I$ and $L_{d2} = L_{q2}$ into (9) yields

$$V_{q2} - V_{d2} = 2RI + \left(D_{Q2} - D_{D2} \right) V_{\rm dead}. \tag{10}$$

Based on (8) and (10), the resistance term is cancelled in

$$\alpha_1 = \omega I_{q1} \left(L_\Delta I_{d1} + \lambda_0 \right) + \kappa_1 V_{\rm dead} \tag{11}$$

where α_1 and κ_1 given in (12) contain only voltage and current measurements that are available. Therefore, α_1 and κ_1 can be calculated from the measurements as follows:

$$\begin{cases} \alpha_1 = \ V_{d1} I_{d1} + V_{q1} I_{q1} \\ \qquad\quad -\gamma I_{s1}^2 \left(V_{q2} - V_{d2} \right) \\ \kappa_1 = \ I_{d1} D_{D1} + I_{q1} D_{Q1} \\ \qquad\quad -\gamma I_{s1}^2 \left(D_{Q2} - D_{D2} \right). \end{cases} \quad \text{with } \gamma = \frac{1}{2I} \tag{12}$$

Proof to (11) and (12): see Appendix.

In (11), λ_0 is PMT dependent, and the rest terms are available, thus one can estimate PMT from (11).

To derive model M2, nonzero testing current I_{q2} will be injected into Q_2 frame. Then, 2nd and 4th equations in (7) are respectively multiplied by I_{q2} and I_{q1}, and the results are

$$V_{q1} I_{q2} = RI_{q1} I_{q2} + \omega I_{q2} (L_{d1} I_{d1} + \lambda_0) + I_{q2} D_{Q1} V_{\rm dead} \tag{13}$$

$$V_{q2} I_{q1} = RI_{q2} I_{q1} + \omega L_{d2} I_{d2} I_{q1} + I_{q1} D_{Q2} V_{\rm dead}. \tag{14}$$

Subtracting (14) from (13) yields

$$\alpha_2 = \omega \left(I_{q2} \left(L_{d1} I_{d1} + \lambda_0 \right) - L_{d2} I_{d2} I_{q1} \right) + \kappa_2 V_{\rm dead} \tag{15}$$

where α_2 and κ_2 in the following can be calculated from measurements.

$$\alpha_2 = V_{q1} I_{q2} - V_{q2} I_{q1}, \quad \kappa_2 = I_{q2} D_{Q1} - I_{q1} D_{Q2}. \tag{16}$$

In M2, a larger I_{q2} will result in a more accurate estimation because V_{q2} increases as the increase of I_{q2}, which leads to an increased signal-to-noise ratio of voltage measurements.

Either (11) or (15) can be employed for PMT estimation, thus two typical estimation models, M1 and M2, will be derived from (11) and (15) accordingly, which will be detailed as follows. It should be noted that one can derive similar models by following the same methodologies.

1) Deriving Estimation Model M1 From (11): Suppose that at time *t*, the PMT is *T*(*t*) and PM flux linkage is $\lambda_T(t)$; the DQ_1 frame currents are $I_{d1,t}$ and $I_{q1,t}$, respectively; the motor speed is ω_t; testing currents are injected into DQ_2 frame, and the measured DQ frame voltages are $V_{d1,t}$, $V_{q1,t}$, $V_{d2,t}$, and $V_{q2,t}$. With these data at time *t*, the following is obtained from (11).

$$\alpha_{1,t} = \omega_t I_{q1,t} \left(L_{\Delta,t} I_{d1,t} + \lambda_T(t) \right) + \kappa_{1,t} V_{\rm dead} \tag{17}$$

$$\begin{cases} \alpha_{1,t} = V_{d1,t} I_{d1,t} + V_{q1,t} I_{q1,t} - \gamma I_{s1,t}^2 \left(V_{q2,t} - V_{d2,t} \right) \\ \kappa_{1,t} = I_{d1,t} D_{D1,t} + I_{q1,t} D_{Q1,t} - \gamma I_{s1,t}^2 \left(D_{Q2,t} - D_{D2,t} \right) \end{cases} \tag{18}$$

where, $\alpha_{1,t}$ and $\kappa_{1,t}$ are obtained by replacing $\{V_{d1}, V_{q1}, V_{d2}, V_{q2}, I_{d1}, I_{q1}\}$ in (12) with $\{V_{d1,t}, V_{q1,t}, V_{d2,t}, V_{q2,t}, I_{d1,t}, I_{q1,t}\}$; $D_{D1,t}$ is the value of D_{D1} at time *t*; similar for $D_{Q1,t}$, $D_{D2,t}$, and $D_{Q2,t}$; $L_{\Delta,t}$ is the value of L_Δ at time *t* and

it can change nonlinearly under different load conditions due to magnetic saturation.

When PMT is within the maximum operating temperature, PM flux linkage decreases linearly as the PMT increases [33], [34]. This linear relationship between PMT and PM flux linkage can be modeled as

$$\lambda_T(t) = \lambda_0 \left(1 + \beta \left(T(t) - T_0\right)\right) \tag{19}$$

where $\lambda_T(t)$ and λ_0 denote the PM flux linkage at temperature $T(t)$ and T_0, respectively, and β is the PM thermal coefficient. For instance, β is $-0.12\%/^{\circ}$C for NdFeB PMs.

Substituting (19) into (17), the result is

$$\frac{\alpha_{1,t} - \kappa_{1,t} V_{\text{dead}}}{\omega_t I_{q1,t}} = L_{\Delta,t} I_{d1,t} + \lambda_0 + \beta\lambda_0 \left(T(t) - T_0\right). \tag{20}$$

In this article, inductances are assumed to be independent from PMT, but they can change nonlinearly under different load conditions due to magnetic saturation. If (20) is employed directly for PMT estimation using the least-squares method, accurate inductances will be required, so the estimation performance will be affected by magnetic saturation. This article employs a look-up-table (LUT) to cancel the inductance terms, so that the proposed estimation approach will not be affected by magnetic saturation.

Suppose that initial tests are conducted at room temperature T_0 and motor speed ω_0 to collect $\{V_{d1,0}, V_{q1,0}, V_{d2,0}, V_{q2,0}\}$ under different DQ_1 frame currents $\{I_{d1,0}, I_{q1,0}\}$ with the same testing currents injected into DQ_2 frame; the PM flux linkage is λ_0 at temperature T_0. In this way, a LUT of $\{V_{d1,0}, V_{q1,0}, V_{d2,0}, V_{q2,0}\}$ with respect to $\{I_{d1,0}, I_{q1,0}\}$ is built. Based on the initial LUT data, the following can be constructed from (11):

$$\alpha_{1,0} - \kappa_{1,0} V_{\text{dead}} = \omega_0 I_{q1,0} \left(L_{\Delta,0} I_{d1,0} + \lambda_0\right) \tag{21}$$

$$\begin{cases} \alpha_{1,0} = V_{d1,0} I_{d1,0} + V_{q1,0} I_{q1,0} - \gamma I_{s1,0}^2 \left(V_{q2,0} - V_{d2,0}\right) \\ \kappa_{1,0} = I_{d1,0} D_{D1,0} + I_{q1,0} D_{Q1,0} - \gamma I_{s1,0}^2 (D_{Q2,0} - D_{D2,0}) \end{cases} \tag{22}$$

where $\alpha_{1,0}$ and $\kappa_{1,0}$ are obtained by replacing $\{V_{d1}, V_{q1}, V_{d2}, V_{q2}, I_{d1}, I_{q1}\}$ in (12) with $\{V_{d1,0}, V_{q1,0}, V_{d2,0}\, V_{q2,0}, I_{d1,0}\, I_{q1,0}\}$, $D_{D1,0}$ is the value of D_{D1} at the initial time; similar for $D_{Q1,0}$ $D_{D2,0}$, and $D_{Q2,0}$, and $L_{\Delta,0}$ is the value of L_{Δ} at the initial time.

The LUT is built under different $I_{d1,0}$ and $I_{q1,0}$ with the same DQ_2 frame currents injected. Hence, it is reasonable to assume that one can find the data from the LUT satisfying the following to construct (21):

$$I_{d1,t} = I_{d1,0}, I_{q1,t} = I_{q1,0} \tag{23}$$

It should be emphasized that even if the LUT does not contain the data satisfying (23), one can obtain the required data through interpolation providing the condition that sufficient data are collected in the LUT.

As discussed in Appendix, D_{D1}, D_{Q1}, D_{D2}, and D_{Q2} are functions of stator currents. From (23), the stator current at time t, $[I_{d1,t}, I_{q1,t}, -I, I]^T$, is equal to the initial one, $[I_{d1,0}, I_{q1,0}, -I, I]^T$, in the LUT, therefore, the following is obtained:

$$\begin{aligned} &D_{D1,0} = D_{D1,t}, D_{Q1,0} = D_{Q1,t}, D_{D2,0} = D_{D2,t} \\ &D_{Q2,0} = D_{Q2,t}, L_{\Delta,0} = L_{\Delta,t}. \end{aligned} \tag{24}$$

Based on (23) and (24), $\kappa_{1,0}$ and $\kappa_{1,t}$ are equal, that is

$$\kappa_{1,0} = \kappa_{1,t}. \tag{25}$$

Substituting (23)$\sim$(25) into (20) and (21) yields

$$\frac{\alpha_{1,t} - \kappa_{1,0} V_{\text{dead}}}{\omega_t I_{q1,t}} = L_{\Delta,t} I_{d1,t} + \lambda_0 + \beta\lambda_0 \left(T(t) - T_0\right) \tag{26}$$

$$\frac{\alpha_{1,0} - \kappa_{1,0} V_{\text{dead}}}{\omega_0 I_{q1,t}} = L_{\Delta,t} I_{d1,t} + \lambda_0. \tag{27}$$

Subtracting (27) from (26) yields the model M1 in (28)

$$\text{M1}: T(t) - T_0 = \frac{\alpha_{1,t} - \frac{\omega_t}{\omega_0}\alpha_{1,0}}{I_{q1,t}\omega_t\beta\lambda_0} + \frac{\omega_t - \omega_0}{\omega_t}\frac{\kappa_{1,0}}{I_{q1,t}}\Delta T \tag{28}$$

where

$$\Delta T = \frac{V_{\text{dead}}}{\omega_0 \beta \lambda_0}. \tag{29}$$

In M1, PMT $T(t)$ is unknown and other parameters are either available in the LUT or can be calculated from the measurements, thus $T(t)$ can be directly estimated from M1.

2) Deriving Estimation Model M2 From (15): Based on the data at time t $\{V_{d1,t}, V_{q1,t}, V_{d2,t}, V_{q2,t}\}$ and the initial LUT data $\{V_{d1,0}, V_{q1,0}, V_{d2,0}, V_{q2,0}\}$, the following can be obtained from (15):

$$\begin{aligned} \frac{\alpha_{2,t} - \kappa_{2,t} V_{\text{dead}}}{\omega_t} &= I_{q2,t} \left(L_{d1,t} I_{d1,t} + \lambda_T(t)\right) \\ &\quad - L_{d2,t} I_{d2,t} I_{q1,t} \end{aligned} \tag{30}$$

$$\frac{\alpha_{2,0} - \kappa_{2,0} V_{\text{dead}}}{\omega_0} = I_{q2,0} \left(L_{d1,0} I_{d1,0} + \lambda_0\right) - L_{d2,0} I_{d2,0} I_{q1,0} \tag{31}$$

Based on (16), $\alpha_{2,0}$, $\kappa_{2,0}$, $\alpha_{2,t}$, and $\kappa_{2,t}$ are given in (32) and the subscript "$_t$" or "$_0$" denotes it is the value of the variable at time t or initial condition. Due to magnetic saturation, $L_{d1,t}$ can be different from $L_{d1,0}$ and $L_{d2,t}$ can be different from $L_{d2,0}$

$$\begin{cases} \alpha_{2,t} = V_{q1,t} I_{q2,t} - V_{q2,t} I_{q1,t}, \\ \alpha_{2,0} = V_{q1,0} I_{q2,0} - V_{q2,0} I_{q1,0} \\ \kappa_{2,t} = I_{q2,t} D_{Q1,t} - I_{q1,t} D_{Q2,t}, \\ \kappa_{2,0} = I_{q2,0} D_{Q1,0} - I_{q1,0} D_{Q2,0}. \end{cases} \tag{32}$$

In the LUT one can find the data satisfying

$$I_{d1,t} = I_{d1,0}, I_{q1,t} = I_{q1,0}. \tag{33}$$

Since the stator current at time t is equal to that at initial condition, the following is obtained

$$\begin{aligned} &D_{D1,0} = D_{D1,t},\ D_{Q1,0} = D_{Q1,t},\ D_{D2,0} = D_{D2,t} \\ &D_{Q2,0} = D_{Q2,t},\ L_{d1,0} = L_{d1,t},\ L_{d2,0} = L_{d2,t}. \end{aligned} \tag{34}$$

Based on (33) and (34), $\kappa_{2,0}$ and $\kappa_{2,t}$ are equal, that is

$$\kappa_{2,0} = \kappa_{2,t}. \tag{35}$$

Substituting (19) and (33)–(35) into (30) and (31), the result is the derived model M2 in the following:

$$\text{M2}: T(t) - T_0 = \frac{\alpha_{2,t} - \frac{\omega_t}{\omega_0}\alpha_{2,0}}{I_{q2,t}\omega_t\beta\lambda_0} + \frac{\omega_t - \omega_0}{\omega_t}\frac{\kappa_{2,0}}{I_{q2,t}}\Delta T. \tag{36}$$

B. Compensation for Inverter Distortion

Both M1 and M2 require the inverter distortion information for PMT estimation, thus it is necessary to analyze how inverter distortion will affect the estimation performance. Ideally, if the LUT is built under all speed conditions, then one can find the data in the LUT satisfying $\omega_0 = \omega_t$. In such a way, is the inverter distortion cancelled as the last term in M1 and M2 becomes zero. However, this will increase the complexity in building the LUT. Therefore, it necessary to compensate or cancel the inference of the inverter distortion.

In M1 and M2, inverter distortion is represented in the form of $\kappa_{1,0}/I_{q1,t}$ and $\kappa_{2,0}/I_{q1,t}$, respectively. As analyzed in the Appendix, D_{D1}, D_{Q1}, D_{D2}, and D_{Q2} are functions of the stator currents, and thus $\kappa_{1,0}$ and $\kappa_{2,0}$ are functions of stator currents as well. In M1 and M2, inverter distortion will be cancelled if $\kappa_{1,0}$ and $\kappa_{2,0}$ become zero. DQ_1 frame currents are determined by load conditions, while DQ_2 frame currents are adjustable. Hence, DQ_2 frame currents should be optimally selected to ensure $\kappa_{1,0}$ satisfying (37) and $\kappa_{2,0}$ satisfying (38) in order to cancel the inverter distortion

$$\text{M1}: \kappa_{1,0} = 0 \Rightarrow \frac{I_{d1,0}D_{D1,0} + I_{q1,0}D_{Q1,0}}{D_{Q2,0} - D_{D2,0}} = \gamma I_{s1,0}^2 \tag{37}$$

$$\text{M2}: \kappa_{2,0} = 0 \Rightarrow I_{q2,0}D_{Q1,0} = I_{q1,0}D_{Q2,0}. \tag{38}$$

Hence, given I_{d1} and I_{q1}, optimal I_{d2} and I_{q2} can be calculated from (37) for M1 and (38) for M2.

According to (22) and (32), calculating $\kappa_{1,0}$ and $\kappa_{2,0}$ involves: 1) obtain N data points of the inverter distorted coefficients $D_{d1,0}$, $D_{q1,0}$, $D_{d2,0}$, and $D_{q2,0}$ in one electrical cycle using (54); 2) compute their average values $D_{D1,0}$, $D_{Q1,0}$, $D_{D2,0}$, and $D_{Q2,0}$ from these data; and 3) calculate $\kappa_{1,0}$ and $\kappa_{2,0}$ using (22) and (32). Hence, the values of $\kappa_{1,0}$ and $\kappa_{2,0}$ are dependent on N. Obviously, N should be as large as possible to ensure the accuracy of calculated $\kappa_{1,0}$ and $\kappa_{2,0}$. In the simulation, N is set to 62 800 to ensure the accuracy. Fig. 2 presents the calculated $\kappa_{1,0}$ and $\kappa_{2,0}$ with respect to DQ_2 frame currents. For $I_{d2} = I_{q2} = I = 0$, there will be no current injection in DQ_2 frame, but M1 requires current injection, thus $\kappa_{1,0}$ has no meaning at $I = 0$. Hence, in Fig. 2(a), (c), and (e), I is set to be within [−5 A, −0.5 A] or [0.5 A, 5 A]. It can be concluded from Fig. 2 that

1) for M1, $\kappa_{1,0}/I_{q1,t}$ decreases with the increase of DQ_2 frame currents, which means that selecting a larger testing current magnitude can reduce the influence of inverter distortion;

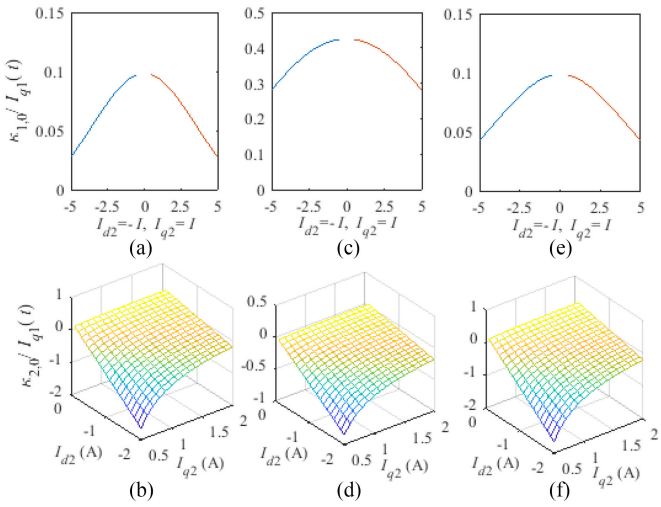

Fig. 2. Investigation of inverter distortion with $N = 62800$. (a) $\kappa_{1,0}/I_{q1}$ and (b) $\kappa_{2,0}/I_{q2}$ for $I_{d1} = -5$ A and $I_{q1} = 8.7$ A. (c) $\kappa_{1,0}/I_{q1}$ and (d) $\kappa_{2,0}/I_{q2}$ for $I_{d1} = -2.6$ A and $I_{q1} = 14.77$ A. (e) $\kappa_{1,0}/I_{q1}$ and (f) $\kappa_{2,0}/I_{q2}$ for $I_{d1} = -6$ A and $I_{q1} = 10.39$ A.

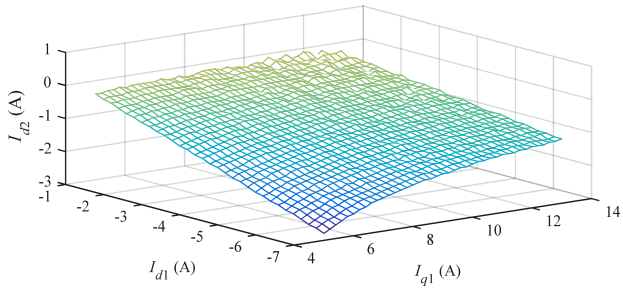

Fig. 3. Optimal I_{d2} for $I_{q2} = 2$ A to cancel the inverter distortion for M2.

2) for M2, with a proper selection of DQ_2 frame currents, (38) can be satisfied, which means that the inference from the inverter distortion can be cancelled.

In most cases, it is unable to find proper I_{d2} and I_{q2} satisfying (37) for M1 because I_{d2} and I_{q2} should remain small as they do not contribute to average torque production. However, one can find proper I_{d2} and I_{q2} satisfying (38) for M2, thus M2 in (36) can be simplified as

$$\text{M2}: T(t) - T_0 = \frac{\alpha_{2,t} - \frac{\omega_t}{\omega_0}\alpha_{2,0}}{I_{q2,t}\omega_t\beta\lambda_0}. \tag{39}$$

Given the DQ_1 frame currents, optimal DQ_2 frame currents to cancel inverter distortion for M2 can be identified from (38). For the test machine, when I_{q2} is set to 2 A, optimal I_{d2} under different I_{d1} and I_{q1} to cancel inverter distortion is calculated and given in Fig. 3. When the test currents in Fig. 3 are injected into DQ_2 frame, inverter distortion can be cancelled for M2 and the temperature can be estimated from (39).

C. Temperature Smoothing Using Kalman Filter

The Kalman filter is employed to smooth the estimated temperatures to reduce the influence from the measurement noise.

PMT variation has a large constant and PMT increase or decrease in a short time period can be approximately viewed as linear. Hence, a linear (40) proposed in [21] is employed to model PMT variation in a short period of time

$$T(t) - T(t-1) = \nu \Delta t \tag{40}$$

where $T(t)$ and $T(t-1)$ denote two consecutive PMTs at time t and $t-1$, respectively; ν denotes the rate of temperature increase or decrease, and Δt denotes the sampling time.

Based on M1, M2 and (40), a state-space model in (41) is constructed for PMT estimation

$$x_{t+1} = \mathbf{A}x_t + g_t, \quad y_t = \mathbf{B}x_t + e_t \tag{41}$$

where x_t, y_t, $\mathbf{A}$ and $\mathbf{B}$, are defined as

$$\begin{cases} \mathbf{A} = [1\ \Delta t;\ 0\ \ 1]\,, \mathbf{B} = [1\ \ 0], x_t = [\,T(t) - T_0\ \ \nu(t)\,]^T \\ y_t = \begin{cases} \dfrac{\omega_0 \alpha_{1,t} - \omega_t \alpha_{1,0}}{I_{q1,t}\omega_0\omega_t\lambda_0\beta} + \dfrac{\omega_t - \omega_0}{\omega_t}\dfrac{\kappa_{1,0}}{I_{q1,t}}\Delta T & \text{for M1} \\ \dfrac{\omega_0 \alpha_{2,t} - \omega_t \alpha_{2,0}}{I_{q2,t}\omega_0\omega_t\beta\lambda_0} & \text{for M2.} \end{cases} \end{cases} \tag{42}$$

Here, g_t and e_t are zero-mean noise with covariances G and E, respectively, where G and E can be selected according to [21].

Since (41) is linear, Kalman filter is employed to estimate PMT, which involves the following four steps: 1) calculate y_t using (42); 2) estimate the state at t using (43); 3) update the state using (44), and y_t; 4) calculate the PMT using (46).

$$\hat{x}_t^- = \mathbf{A}\hat{x}_{t-1} \tag{43}$$

$$\hat{x}_t = \hat{x}_t^- + K_t(y_t - \mathbf{B}\hat{x}_t^-) \tag{44}$$

$$\begin{cases} K_t = P_t^-\mathbf{B}^T(\mathbf{B}P_t^-\mathbf{B}^T + E)^{-1} \\ P_t^- = \mathbf{A}P_{t-1}\mathbf{A}^T + G,\ P_t = P_t^- - K_t\mathbf{B}P_t^- \end{cases} \tag{45}$$

$$\hat{T}(t) = \hat{x}_t(1) + T_0 \tag{46}$$

where $\hat{x}_t^-$ and $\hat{x}_t$ are predicted and estimated states at time t.

D. Discussion on Machine Model Uncertainties

This article assumes that machine structure is symmetrical and winding distribution is sinusoidal with harmonics and iron loss neglected. This subsection discusses how harmonics, iron loss, and asymmetrical structure will affect the estimation performance.

The winding function harmonics can result in harmonics in the inductances in DQ frames. According to [32], DQ frame inductance matrix $\mathbf{L}_{\mathrm{DQ}}$ in (47) is calculated from $\mathbf{T}_{\mathrm{DQ}}\mathbf{L}\mathbf{T}_{\mathrm{DQ}}^{-1}$

$$\mathbf{L}_{\mathrm{DQ}} = \begin{bmatrix} L_{d1} & L_{d1q1} & L_{d1d2} & L_{d1q2} \\ L_{d1q1} & L_{q1} & L_{q1d2} & L_{q1q2} \\ L_{d1d2} & L_{q1d2} & L_{d2} & L_{d2q2} \\ L_{d1q2} & L_{q1q2} & L_{d2q2} & L_{q2} \end{bmatrix} \tag{47}$$

where L_x and L_{xy} are the self and mutual inductances with $x \in \{d_1, q_1, d_2, q_2\}$ and $xy \in \{d_1q_1, d_1d_2, d_1q_2, q_1d_2, q_1q_2, d_2q_2\}$

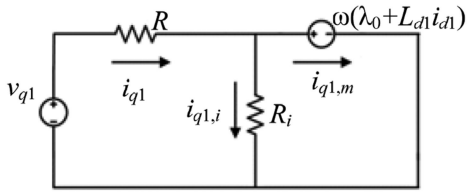

Fig. 4. Equivalent circuit of Q_1 frame considering iron loss.

and $L_{xy} = L_{yx}$. In (47), L_x and L_{xy} can be expressed as [32]

$$L_x = L_{x,0} + \sum\nolimits_j L_{x,j}, \quad L_{xy} = \sum\nolimits_j L_{xy,j} \tag{48}$$

where $L_{x,0}$ is the dc component of L_x and $L_{\mathrm{x},j}$ is the jth harmonic component in L_x with $j = 6, 12, \ldots$; $L_{xy,j}$ is the jth harmonic component in L_{xy} with $j = 6, 12, \ldots$.

According to (3), the inductance harmonics will produce the voltage harmonics of the same order. However, this article employs dc values for temperature estimation, so the induced voltage harmonics will be averaged to zero and will not affect the estimation performance.

According to [32], DQ_1 frame PM flux linkages λ_{d1} and λ_{q1} contain dc and kth harmonic components and DQ_2 frame PM flux linkages λ_{d2} and λ_{q2} contain the lth harmonics, with $k = 12, 24, 36, \ldots$ and $l = 6, 18, 30, \ldots$, which can be denoted as

$$\begin{cases} \lambda_{d1} = \lambda_0 + \sum_k \lambda_{dk,1},\ \lambda_{q1} = \sum_k \lambda_{qk,1} \\ \lambda_{d2} = \sum_l \lambda_{dl,2}, \qquad \lambda_{q2} = \sum_l \lambda_{ql,2} \end{cases} \tag{49}$$

where λ_0 is the fundamental component, $\lambda_{dk,1}$ and $\lambda_{qk,1}$ are the kth harmonic components in DQ_1 frame, and $\lambda_{dl,1}$ and $\lambda_{ql,1}$ are the lth harmonic components in DQ_2 frame. Similarly, PM flux linkage harmonics will introduce voltage harmonics with the same order, but these harmonic components will be averaged to zero and thus will not affect the estimation performance.

When the iron loss is considered, iron loss resistances can be inserted in parallel with the armature inductances in DQ frame equivalent circuits [37]. Fig. 4 presents an equivalent circuit in Q_1 frame considering iron loss, which is based on the circuits in [37]. According to [37], the iron loss resistance R_i is significantly larger than the impedance ωL_{q1}. Therefore, in Fig. 4, Q_1 frame magnetizing current $i_{q1,m}$ will be slightly smaller than Q_1 frame line current i_{q1}, which will affect the estimation performance, but the influence is not significant as will be seen in experimental results. In order to improve the estimation performance, future work is required to investigate iron loss modeling and compensation for DT-PMSM.

According to [38], the machine with asymmetrical structure has unbalanced phase winding impedances, which will lead to positive, negative and zero sequence components in the voltage, current, and flux linkages (zero sequence components will be zero for the machine with floating neutral points). The asymmetrical structure can result in the second order torque and flux harmonics [38]. The flux harmonics will not affect the proposed approach as discussed above. However, the induced negative sequence components could affect the estimation performance especially for severely asymmetrical machine, which requires

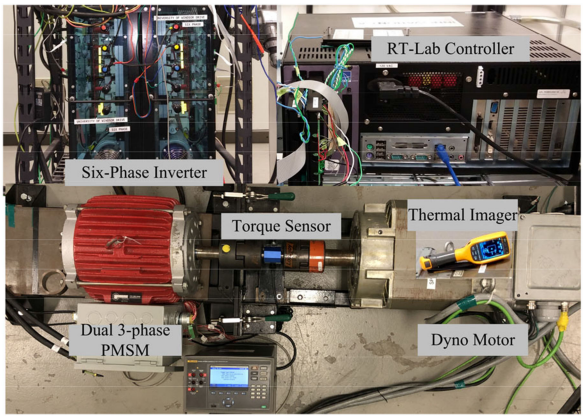

Fig. 5. Experimental setup for PMT estimation.

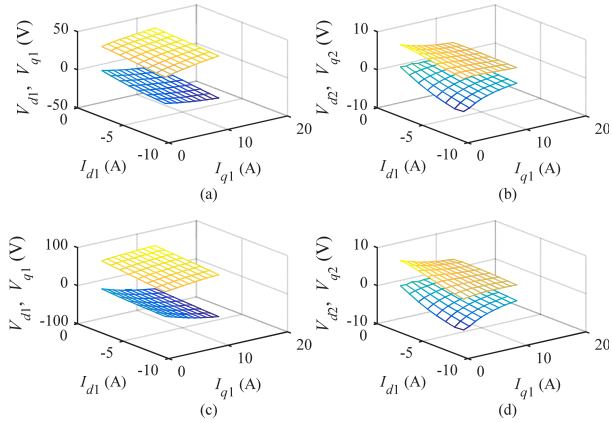

Fig. 6. LUTs built at 100 and 300 r/min for M2. (a) DQ_1 frame voltages at 100 r/min. (b) DQ_2 frame voltages at 100 r/min. (c) DQ_1 frame voltages at 300 r/min. (d) DQ_2 frame voltages at 300 r/min.

TABLE I
DESIGN PARAMETERS OF THE TEST DT-PMSM

Rated current	15 A	NO. of pole pairs/slots	4/48
Rated torque	75 Nm	Resistance	0.5 Ω
Rated speed	575 rpm	PM flux linkage	0.339 Wb·turn
L_{d1}@ I_s=15 A,γ=30°	12.5 mH	L_{q1}@I_s=15 A,γ=30°	33.4 mH
L_{d2}@I_{d2}=0, I_{q2}=0	1.7 mH	L_{q2}@I_{d2}=0, I_{q2}=0	1.7 mH
DC Link Voltage	250 V	Switching frequency	10 kHz
Sampling time	2.5 μs	Dead time	1 μs

future work on accurate modeling and compensation of the asymmetrical machine structure.

IV. EXPERIMENTAL INVESTIGATIONS

A. Experimental Setup and Preliminary Test

The proposed approach is applied to estimate the PMT of a laboratory interior DT-PMSM, as shown in Fig. 5. Table I lists the design parameters of the test motor drive. For the test motor, there are thermocouple installed inside the winding for temperature measurement and windows on the surface, as shown in Fig. 5. Through these windows, PMT can be measured by using a thermal imager, the measured PMT is the surface temperature and the temperature distribution is nonuniform. The estimated PMT from PM flux linkage can be viewed as the average value. Although the measured PMT is not exactly equal to the average value, but that their difference is not significant, so the measured PMT will be compared with the estimated ones to evaluate the estimation performance of the proposed approach.

To perform PMT estimation, the first step is to build the LUT. In particular, the LUT is built for two speeds, namely, 100 and 300 r/min. In building the LUT for M1, DQ_2 frame current magnitude is experimentally selected to be 2 A; in building the LUT for M2, optimal DQ_2 frame currents in Fig. 3 are selected. The LUTs built for M2 at 100 and 300 r/min are shown in Fig. 6 and the ones for M1 are similar. With these LUTs, PMT can be estimated from real-time measurements.

B. Experimental Parameter Estimation Results

To evaluate the proposed approach, four tests, Test 1, Test 2, Test 3, and Test 4 are conducted under various speed and load conditions. Specifically, Test 1 is conducted at a low speed of 100 r/min with a load torque of 68 Nm; Test 2 is conducted at a higher speed of 300 r/min with a load torque of 66.5 Nm; Test 3 is conducted under various speed and load conditions, in which the load torque is 66.5 Nm and the speed is 400 r/min in the first hour, and then the load torque and speed are decreased to 48.5 Nm and 200 r/min, respectively, and the load torque is further reduced to 21 Nm after 80 minutes; and Test 4 is conducted under four different loads and two speeds in a short period of time. According to (7), the voltage drop due to PM flux linkage is proportional to the speed. This means that the higher the speed is, the higher the signal-to-noise ratio of the measurements will be. Therefore, the estimation performance at higher speeds is generally better than that at low speeds. Hence, experiments are mainly conducted below rated speed. The tests are conducted in an open laboratory space, so tests 1∼3 are conducted for a long period in order for the motor to reach a high temperature, In tests 1∼3, temperature estimation is performed every one minute as temperature variation has a large time constant, thus the test current injection in DQ_2 frame is at the same rate and each time DQ_2 frame currents are injected for a duration of one second (this duration can be shorter for the high-speed conditions, and one second is used here to cover very low-speed conditions). For machine control, the sampling time is 2.5 μs, but a down-sampling factor of 40 is employed to achieve a lower sampling rate of 1 kHz to collect the data for temperature estimation, so there will be 1 000 data points for each variable and the arithmetic mean of these data are used as the dc values for temperature estimation.

In Test 1, the motor is running at 100 r/min and 68 Nm with $I_{d1} = -6$ A and $I_{q1} = 13$ A. During PMT estimation, the measurements will be taken after I_{d2} and I_{q2} are injected, and they are set to zero after data collection. Test 1 is conducted for about one hour to increase the PMT. During this test, the thermal imager is employed to measure the PMT per 20 min. It should be noted that the measured PMT during standstill is accurate, but the ones measured during operation has limited accuracy due to the rotation of PMs. Winding temperature is monitored by

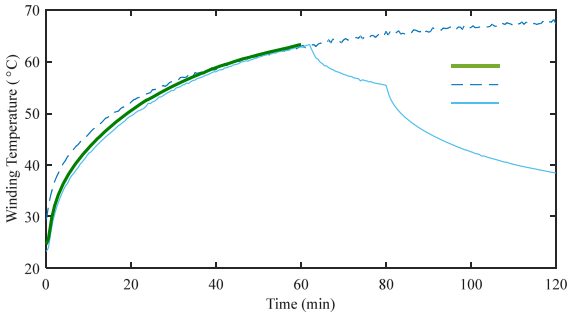

Fig. 7. Winding temperatures during Test 1, Test 2, and Test 3.

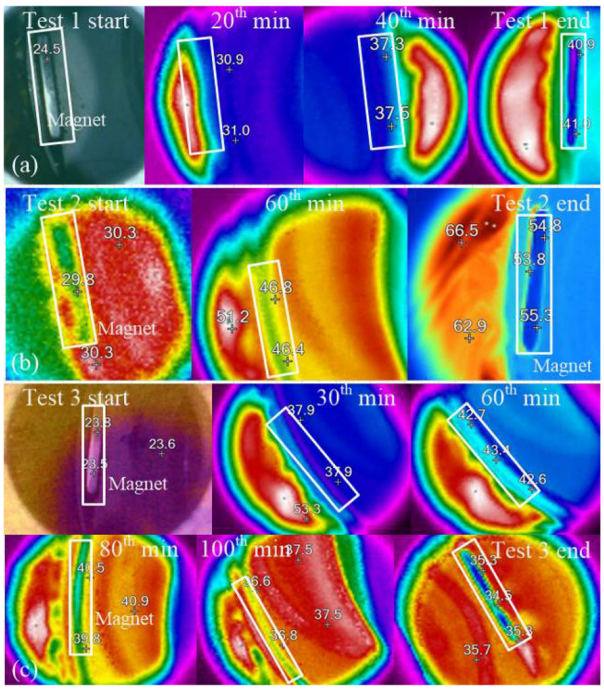

Fig. 8. Measured thermal images (unit: °C). (a) Test 1. (b) Test 2. (c) Test 3.

thermocouple, and measured temperature in Test 1 is shown in Fig. 7. The measured thermal images are presented in Fig. 8(a). In Fig. 8, the thermal image was taken from a slightly different angle each time to capture the PM resulting in difference in the image shape. In Fig. 8, both the coil and PMTs are measured, and winding temperature is generally higher than PMT. From Figs. 7 and 8(a), initial winding temperature is 24.5 °C, which is equal to PMT. In the end, winding and PMTs reach 64 and 41 °C, respectively.

In Test 1, the measured speed, currents and voltages are shown in Fig. 9. With these data, the estimated PMT is shown in Fig. 10, in which the measured PMTs and the estimated ones using M1 and M2 without Kalman filter are also compared. The parameters of Kalman filter used are as follows. The covariance G depends on the maximum temperature variation within Δt. Here, Δt is 1 minute and G is selected to be $[2^2\ 0; 0\ 1]$. The covariance E depends on the variation of y_t within Δt. E is experimentally selected to be 2^2. From Fig. 10, at the beginning, 20th and 40th

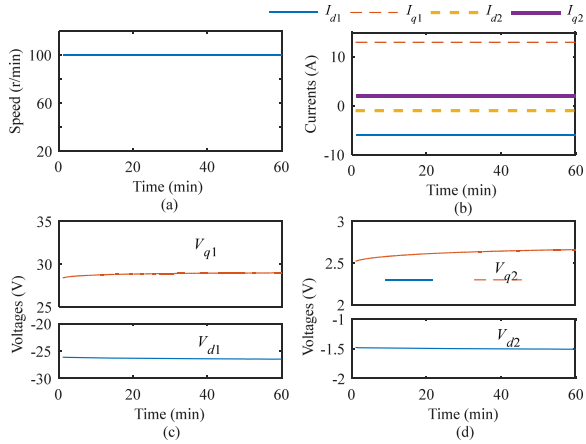

Fig. 9. Measurements in Test 1. (a) Speed. (b) Currents. (c) DQ_1 frame voltages. (d) DQ_2 frame voltages.

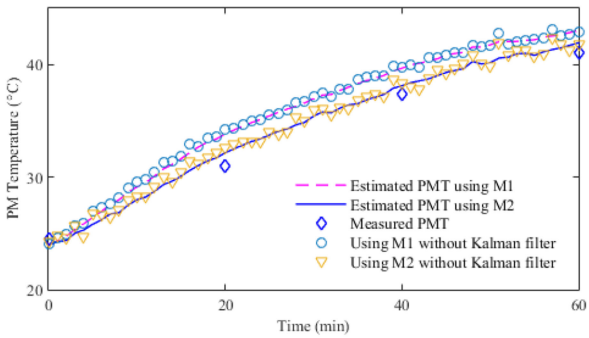

Fig. 10. PMT estimation result in Test 1.

minute and the end of Test 1, the estimated PMT based on M1 is 24.3, 33.8, 39.7, and 43 °C, respectively, the estimated ones based on M2 are 24.2, 32.2, 38.2, and 41.9 °C, respectively, while the measured one is 24.5, 31, 37.4, and 41 °C, respectively. It can be seen that the estimation error is within 3 °C by using M1 and it is within 1.5 °C by using M2. Moreover, Fig. 10 shows that using Kalman filter can help to smooth the estimated temperature to reduce the influence from measurement noise.

In Test 2, the motor is running at 300 r/min with $I_{d1} = -7$ A and $I_{q1} = 12$ A. In order to perform PMT estimation, I_{d2} and I_{q2} are injected into the machine. Test 2 lasts about two hours, and the winding temperature and measured thermal images are presented in Figs. 7 and 8(b), respectively. It can be seen that temperature rise in the first hour is more significant than that in the next hour, and the winding and PMT are 30 °C at the beginning and they are 68 and 55 °C, at the end of Test 2.

The measurements collected during Test 2 are shown in Fig. 11, and the estimated PMT based on M2 is shown in Fig. 12, in which the measured temperatures are compared. From Fig. 12, the estimated PMT is 29 °C at the beginning and 56.5 °C at the end, while the measured one is 30 °C at the beginning and 55 °C at the end. It should be noted that at the 60th minute, it becomes challenging to accurately measure the PMT from the thermal image due to the fast rotation of PMs. In fact, the measured temperature in Fig. 8(b) is close to the

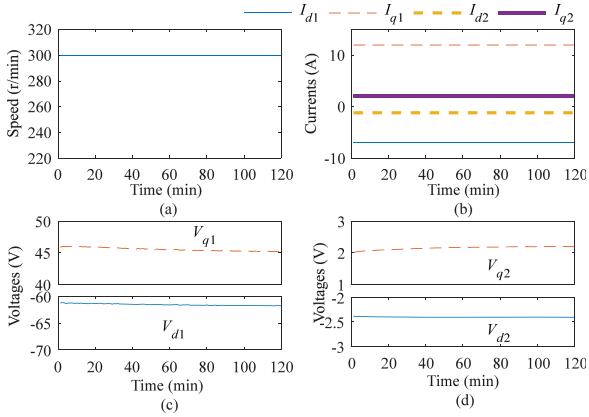

Fig. 11. Measurements in Test 2. (a) Speed. (b) Currents. (c) DQ_1 frame voltages. (d) DQ_2 frame voltages.

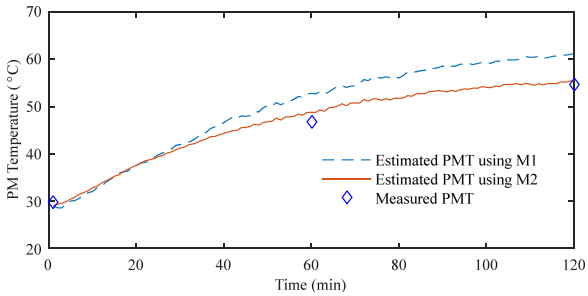

Fig. 12. PMT estimation result in Test 2.

rotor temperature. For comparison purpose, this temperature is regarded as the PMT, but the estimation error at the 60th minute is less than 2.8 °C as shown in Fig. 12. At the end, the estimation error is 1.5 °C. Hence, the proposed approach is capable of effective PMT estimation. In Fig. 12, the estimated PMT based on M1 is also compared. It can be observed from Fig. 12 that the maximum estimation errors for M1 and M2 are 5.4 and 2.8 °C, respectively, thus the M2 can achieve a better accuracy than M1, which confirms with result in Test 1. This is mainly due to two reasons. First, inverter distortion is compensated for M1, while it is cancelled for M2. Therefore, any error in the parameters used for compensating inverter distortion (e.g., $V_{\rm dead}$) can affect the estimation performance using M1, but it will not affect the estimation performance using M2. On the other hand, in M1, V_{d1}, V_{q1}, V_{d2}, and V_{q2} are used, but in M2 only V_{q1} and V_{q2} are used. From (7), PMT variation will lead to the change of V_{q1}, and the use of other voltages is to eliminate the winding resistance. For M1, the use of V_{d1}, V_{d2} and V_{q2} will result in the fact that the measurement noise and model uncertainty from D_1, D_2, and Q_2 frames will be introduced to affect the estimation performance. However, for M2, the use of V_{q1} and V_{q2} can avoid the influence from D_1 and D_2 frames. Hence, M2 can achieve better accuracy and it will be used for PMT estimation in Test 3 and Test 4.

In Test 3, the motor speed is first set to 400 r/min and then reduced to 200 r/min at the 60th minute, while the load torque is 66.5 Nm and reduced to 48.5 and 21 Nm at 60th and 80th minute

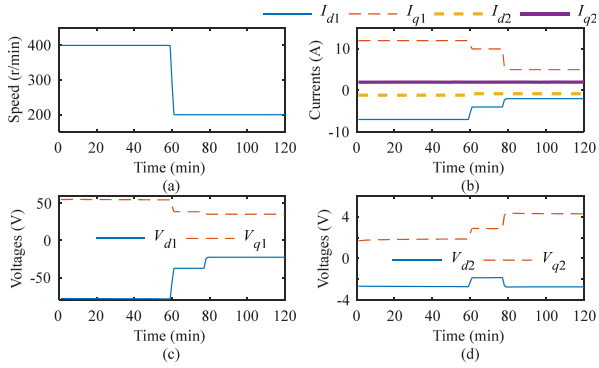

Fig. 13. Measurements in Test 3. (a) Speed. (b) Currents. (c) DQ_1 frame voltages. (d) DQ_2 frame voltages.

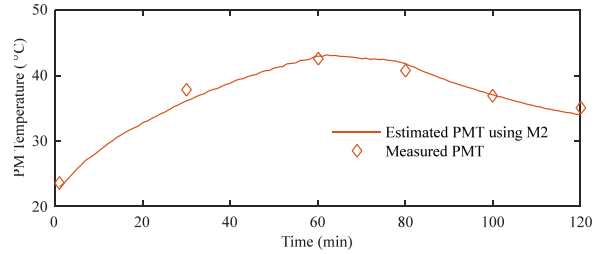

Fig. 14. PMT estimation result in Test 3.

TABLE II
OPERATING CONDITIONS CONSIDERED IN TEST 4

Condition	I_{d1} (A)	I_{q1} (A)	Speed (r/min)
1	-1	8	200, 400
2	-4	10	200, 400
3	-6	11	200, 400
4	-6	13	200, 400

respectively. As can be seen in Fig. 7, in the first hour, the load torque is the same as that in Test 2, but the winding temperature rise is more significant in Test 3, which is due to the increase of motor losses at a higher speed. The measured thermal images are shown in Fig. 8(c), which shows that the PMT is 24 °C at beginning and 35 °C at the end.

The measurements are shown in Fig. 13, and the estimated PMT is compared with the measured one in Fig. 14. The PMT increases in the first hour and then decreases due to the reduction of load torque. Moreover, when the load torque is reduced from 48.5 to 21 Nm, the temperature decrease rate is increased, which is due to the further reduction in motor loss. As can be seen from Figs. 7 and 14, the variation of PMT follows similar trend as that of the winding temperature, and the estimation error is 0.6 °C at the beginning, 1.8 °C at 30th minute, and 0.4 °C at 60th minute, 1.1 °C at 80th minute, and 1 °C at the end. The estimation error is less than 2 °C, thus the proposed approach can achieve accurate PMT estimation under various operating conditions.

In Test 4, four load conditions and two speeds are considered as listed in Table II for temperature estimation in a short time period. In this test, the motor speeds and load conditions are measured and presented in Fig. 15, and the measured PMT is

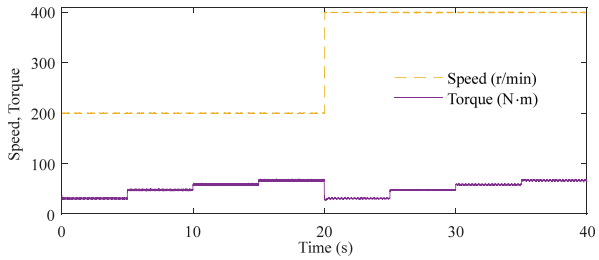

Fig. 15. Measured speed and torque in Test 4.

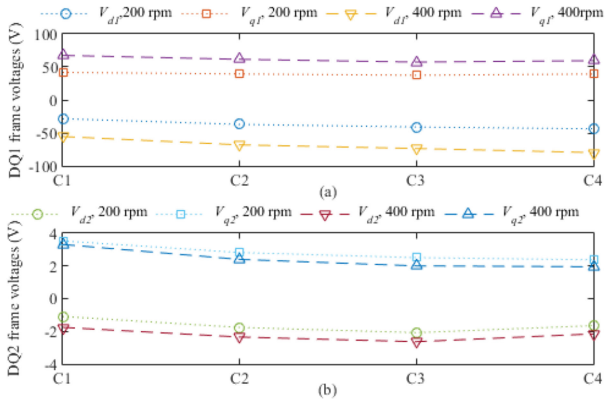

Fig. 16. DQ frame voltages with DQ_2 frame currents injected in Test 4.

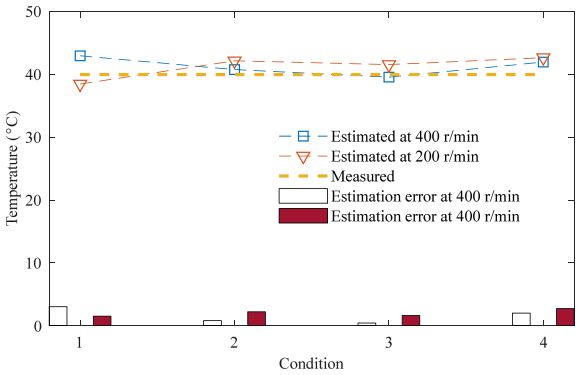

Fig. 17. PMT estimation results in Test 4.

40 °C. In order to estimate the PMT, the optimal DQ_2 frame currents in Fig. 3 are injected for each condition, and the corresponding DQ_1 and DQ_2 frame voltages are presented in Fig. 16. The estimated temperatures using M2 are shown in Fig. 17. The estimation error under each condition is less than 5 °C, thus the proposed approach can accurately estimate PMT under different operating conditions.

C. Discussions on Voltage Variation and Torque Ripple

During motor operation, DQ_1 frame currents are determined by the load condition with a particular control strategy such as maximum torque per ampere (MTPA) control, while DQ_2 frame currents are selected to reduce/cancel the influence of inverter distortion as discussed in Section III.B. From (7) V_{q1}

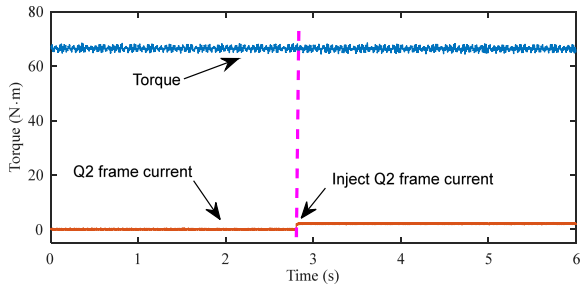

Fig. 18. Output torque with and without DQ_2 frame current injection.

is dependent on both the winding and PMT, while V_{d1}, V_{d2}, and V_{q2} are dependent on winding temperature. For a particular operating condition, as winding temperature increases, R will increase, so V_{d1}, V_{d2}, and V_{q2} will increase as well. However, V_{q1} is dependent on both winding and PMT, so its variation is analyzed as follows. In (7), RI_{q1} increases as winding temperature increases, while $\omega\lambda_0$ decreases as PMT increases. During motor operation, both winding and PMT will increase, so the variation of V_{q1} is dependent on the variation of $RI_{q1} + \omega\lambda_0$. At a low speed of 100 r/min, V_{q1} in Fig. 9 increases as winding temperature increases because the increase of RI_{q1} is larger than the decrease of $\omega\lambda_0$; while at a high speed of 300 r/min, V_{q1} in Fig. 11 decreases as PMT increases because the increase of RI_{q1} is smaller than the decrease of $\omega\lambda_0$.

The output torque of the test motor before and after current injection in DQ_2 frame is compared in Fig. 18. It can be seen that the injected currents have a negligible influence on the torque ripple. The reason is as follows. According to [32], DQ_2 frame PM flux linkages contain only harmonic components, which will interact with the injected DQ_2 frame currents to produce the torque ripple. However, the magnitudes of the injected currents and PM flux linkage harmonics are both small, and thus the induced torque ripple is negligible.

V. Conclusion

In this article, two estimation models are derived for DT-PMSM PMT estimation based on current injection, in which there is no need of resistance and inductances and the estimation performance is independent from parameter variation. Since currents are injected into DQ_2 frame and the magnitudes of which are small, so the induced machine loss is negligible. For instance, in Test 2, the copper loss due to the injected current occupies less than 0.1% of the machine output power, thus the proposed approach has a negligible influence on the machine efficiency. Moreover, the current injection is performed in a short period, and the injected currents will be controlled back to zero after data collection. Experimental results demonstrate that estimation model M2 can achieve a better estimation performance owing to the cancellation of inverter distortion, while the model M1 can achieve satisfactory estimation accuracy. The proposed approach requires offline tests to construct the LUT and additional memory to store it. One can store α instead of all the current and voltage measurements, which can reduce the LUT size and computation required in the temperature estimation.

The LUT plays an important role in cancelling the inductance term in the proposed models and improving the robustness of the proposed approach to magnetic saturation.

APPENDIX

According to [35], [36], the inverter voltage distortion on the phase voltage can be denoted as

$$\Delta V = [\Delta v_a \quad \Delta v_b \quad \Delta v_c \quad \Delta v_x \quad \Delta v_y \quad \Delta v_z]^T \tag{50}$$

where Δv_x denotes the distorted voltage on the phase x and $\Delta v_x = V_{\text{dead}}\,\text{sign}(i_x)$, where $x = a, b, c, x, y$ or z and V_{dead} denotes the distorted coefficient due to the deadtime effect.

The inverter voltage distortion in DQ frame can be calculated from the phase distorted voltages by applying the transformation matrix $\mathbf{T}_{\text{DQ}}$ to (50), which is

$$\begin{aligned}\Delta V_{\text{DQ}} &= \mathbf{T}_{\text{DQ}}\Delta V \\ &= V_{\text{dead}}\mathbf{T}_{\text{DQ}}\text{sign}\left([i_a \quad i_b \quad i_c \quad i_x \quad i_y \quad i_z]^T\right).\end{aligned} \tag{51}$$

Comparing (51) with (5), the inverter distorted coefficients can be calculated from

$$[D_{d1} \quad D_{q1}D_{d2} \quad D_{q2}]^T = \mathbf{T}_{\text{DQ}}\text{sign}([i_a \quad i_b \quad i_c \quad i_x \quad i_y \quad i_z]^T). \tag{52}$$

Substituting $[i_a\ i_b\ i_c\ i_x\ i_y\ i_z] = \mathbf{T}_{\text{DQ}}^{-1}\mathbf{I}_{\text{DQ}}$ with $\mathbf{I}_{\text{DQ}} = [i_{d1}\ i_{q1}\ i_{d2}\ i_{q2}]^T$ into (52) yields

$$[D_{d1} \quad D_{q1} \quad D_{d2} \quad D_{q2}]^T = \mathbf{T}_{\text{DQ}}\text{sign}(\mathbf{T}_{\text{DQ}}^{-1}\mathbf{I}_{\text{DQ}}). \tag{53}$$

Here $\mathbf{T}_{\text{DQ}}^{-1}$ is the inverse of $\mathbf{T}_{\text{DQ}}$. Based on (53), $D_{d1}, \ldots, D_{q2}$ can be calculated from

$$\begin{cases} D_{d1} = \mathbf{T}_{\text{DQ}}(:,1)\text{sign}(\mathbf{T}_{\text{DQ}}^{-1}\mathbf{I}_{dq}) \\ D_{q1} = \mathbf{T}_{\text{DQ}}(:,2)\text{sign}(\mathbf{T}_{\text{DQ}}^{-1}\mathbf{I}_{dq}) \\ D_{d2} = \mathbf{T}_{\text{DQ}}(:,3)\text{sign}(\mathbf{T}_{\text{DQ}}^{-1}\mathbf{I}_{dq}) \\ D_{q2} = \mathbf{T}_{\text{DQ}}(:,4)\text{sign}(\mathbf{T}_{\text{DQ}}^{-1}\mathbf{I}_{dq}) \end{cases} \tag{54}$$

where $\mathbf{T}_{\text{DQ}}(:, i)$ denotes the ith row of $\mathbf{T}_{\text{DQ}}$, $i = 1, 2, 3, 4$. From (54), $D_{d1}, \ldots, D_{q2}$ are functions of rotor position and stator currents, and for a given $\mathbf{I}_{\text{DQ}}$ they are functions of only rotor position. The expressions of $D_{d1}, \ldots, D_{q2}$ for $i_{d2} = i_{q2} = 0$ are given in [28], [35], which demonstrates that they are periodical functions of the rotor position.

Fig. 19 presents $D_{d1}, \ldots, D_{q2}$ with respect to the rotor position under four different $\mathbf{I}_{\text{DQ}}$, in which there are $N = 6280$ data points for each waveform for demonstration. It can be observed from Fig. 19 that $D_{d1}, \ldots, D_{q2}$ are periodical functions of rotor position for a given $\mathbf{I}_{\text{DQ}}$, which agrees with above analysis and results in other references. Hence, when the average values are calculated by using the data points from one electrical cycle, $D_{D1}, \ldots, D_{Q2}$ will be independent from the rotor position. Given an $\mathbf{I}_{\text{DQ}}$, $D_{d1}, \ldots, D_{q2}$ are periodical functions of rotor position, so their averages can be calculated by using the data points from one electrical cycle in Fig. 19.

From (54), $D_{d1}, \ldots, D_{q2}$ are independent from the deadtime T_{dead}. However, the distorted voltage V_{dead} is dependent on

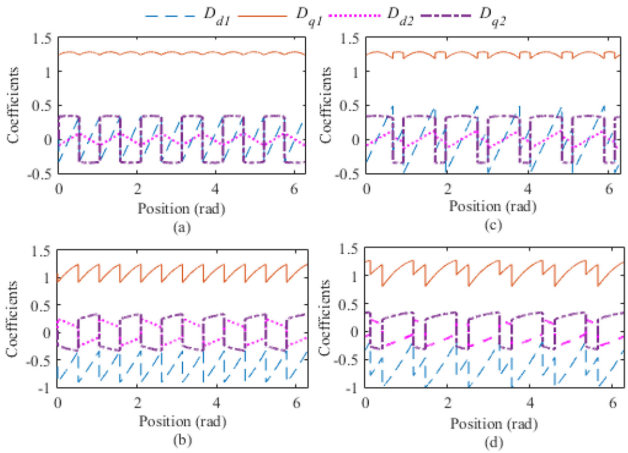

Fig. 19. D_{d1}, D_{q1}, D_{d2} and D_{q2} with respect to the rotor position for a given $\mathbf{I}_{\text{DQ}}$ (unit: A). (a) $\mathbf{I}_{\text{DQ}} = [0\ 10\ 0\ 0]^T$. (b) $\mathbf{I}_{\text{DQ}} = [-5\ 8.67\ 0\ 0]^T$. (c) $\mathbf{I}_{\text{DQ}} = [0\ 15\ 0\ 2]^T$. (d) $\mathbf{I}_{\text{DQ}} = [-7.5\ 12.99\ 0\ 2]^T$.

T_{dead}, and according to [39], V_{dead} can be calculated from

$$V_{\text{dead}} = 0.25\left((T_{\text{off}} - T_{\text{on}} - T_{\text{dead}})V_{\text{dc}} - 2V_{ce0} - 2V_{d0}\right) \tag{55}$$

where T_{on} and T_{off} are the turn-ON and turn-OFF time delays of the switches, respectively; V_{ce0} and V_{d0} are the threshold voltages of the active switch and the freewheeling diode, respectively, and V_{dc} is the dc bus voltage. In this article, V_{dead} is experimentally estimated to be 0.5 V.

Proof to (11) and (12): R can be obtained from (10) as

$$R = \gamma\left(V_{q2} - V_{d2} - (D_{Q2} - D_{D2})\,V_{\text{dead}}\right). \tag{56}$$

Substituting R in (56) into (8), the result is

$$\begin{aligned}V_{d1}I_{d1} + V_{q1}I_{q1} &= \gamma\left(V_{q2} - V_{d2} - (D_{Q2} - D_{D2})\,V_{\text{dead}}\right)I_{s1}^2 \\ &+ \omega I_{q1}\left(L_\Delta I_{d1} + \lambda_0\right) + \left(I_{d1}D_{D1} + I_{q1}D_{Q1}\right)V_{\text{dead}}\end{aligned} \tag{57}$$

Equation (57) can be reorganized as

$$\alpha_1 = \omega I_{q1}\left(L_\Delta I_{d1} + \lambda_0\right) + \kappa_1 V_{\text{dead}} \tag{58}$$

where α_1 and κ_1 are in (12). Hence, (11) and (12) are derived.

REFERENCES

[1] F. Barrero and M. J. Duran, "Recent advances in the design, modeling, and control of multiphase machines—Part I," *IEEE Trans. Ind. Electron.*, vol. 63, no. 1, pp. 449–458, Jan. 2016.

[2] X. Wang, Z. Wang, Z. Xu, J. He, and W. Zhao, "Diagnosis and tolerance of common electrical faults in t-type three-level inverters fed dual three-phase PMSM drives," *IEEE Trans. Power Electron.*, vol. 35, no. 2, pp. 1753–1769, Feb. 2020.

[3] X. Wang, Z. Wang, Z. Xu, M. Cheng, W. Wang, and Y. Hu, "Comprehensive diagnosis and tolerance strategies for electrical faults and sensor faults in dual three-phase PMSM drives," *IEEE Trans. Power Electron.*, vol. 34, no. 7, pp. 6669–6684, Jul. 2019.

[4] Y. Luo and C. Liu, "A simplified model predictive control for a dual three-phase PMSM with reduced harmonic currents," *IEEE Trans. Ind. Electron.*, vol. 65, no. 11, pp. 9079–9089, Nov. 2018.

[5] S. Hu, Z. Liang, W. Zhang, and X. He, "Research on the integration of hybrid energy storage system and dual three-phase PMSM drive in EV," *IEEE Trans. Ind. Electron.*, vol. 65, no. 8, pp. 6602–6611, Aug. 2018.

[6] M. J. Duran and F. Barrero, "Recent advances in the design, modeling, and control of multiphase machines—Part II," *IEEE Trans. Ind. Electron.*, vol. 63, no. 1, pp. 459–468, Jan. 2016.
[7] Z. Wang, X. Wang, M. Cheng, and Y. Hu, "Comprehensive investigation on remedial operation of switch faults for dual three-phase PMSM drives fed by T-3L inverters," *IEEE Trans. Ind. Electron.*, vol. 65, no. 6, pp. 4574–4587, Jun. 2018.
[8] W. Wang, J. Zhang, M. Cheng, and S. Li, "Fault-tolerant control of dual three-phase permanent-magnet synchronous machine drives under open-phase faults," *IEEE Trans. Ind. Electron.*, vol. 32, no. 3, pp. 2052–2063, Mar. 2017.
[9] G. Feng, C. Lai, W. Li, J. Tjong, and N. C. Kar, "Open-phase fault modeling and optimized fault tolerant control of dual three-phase permanent magnet synchronous machines," *IEEE Trans. Power Electron.*, vol. 34, no. 11, pp. 11116–11127, Nov. 2019.
[10] Y. Hu, Z. Q. Zhu, and M. Odavic, "Torque capability enhancement of dual three-phase PMSM drive with fifth and seventh current harmonics injection," *IEEE Trans. Ind. Appl.*, vol. 53, no. 5, pp. 4526–4535, Sep./Oct. 2017.
[11] Z. H. Liu, H. L. Wei, X. H. Li, K. Liu, and Q. C. Zhong, "Global identification of electrical and mechanical parameters in PMSM drive based on dynamic self-learning PSO," *IEEE Trans. Power Electron.*, vol. 33, no. 12, pp. 10858–10871, Dec. 2018.
[12] O. Wallscheid, A. Specht, and J. Böcker, "Observing the permanent-magnet temperature of synchronous motors based on electrical fundamental wave model quantities," *IEEE Trans. Ind. Electron.*, vol. 64, no. 5, pp. 3921–3929, May 2017.
[13] D. Fernandez *et al.*, "Permanent magnet temperature estimation in pm synchronous motors using low cost hall effect sensors," *IEEE Trans. Ind. Appl.*, vol. 53, no. 5, pp. 4515–4525, Sep./Oct. 2017.
[14] C. Kral, A. Haumer, and S. B. Lee, "A practical thermal model for the estimation of permanent magnet and stator winding temperatures," *IEEE Trans. Power Electron.*, vol. 29, no. 1, pp. 455–464, Jan. 2014.
[15] D. Staton and A. Cavagnino, "Convection heat transfer and flow calculations suitable for electric machines thermal models," *IEEE Trans. Ind. Electron.*, vol. 55, no. 10, pp. 3509–3516, Oct. 2008.
[16] G. Demetriades, H. Parra, E. Andersson, and H. Olsson, "A real-time thermal model of a permanent-magnet synchronous motor," *IEEE Trans. Power Electron.*, vol. 25, no. 2, pp. 463–474, Feb. 2010.
[17] D. Reigosa, D. Fernandez, T. Tanimoto, T. Kato, and F. Briz, "Comparative analysis of BEMF and pulsating high-frequency current injection methods for PM temperature estimation in PMSMs," *IEEE Trans. Power Electron.*, vol. 32, no. 5, pp. 3691–3699, May 2017.
[18] K. Liu, J. Feng, S. Guo, L. Xiao, and Z. Q. Zhu, "Identification of flux linkage map of permanent magnet synchronous machines under uncertain circuit resistance and inverter nonlinearity," *IEEE Trans. Ind. Inform.*, vol. 14, no. 2, pp. 556–568, Feb. 2018.
[19] K. Liu and Z. Q. Zhu, "Online estimation of the rotor flux linkage and voltage-source inverter nonlinearity in permanent magnet synchronous machine drives," *IEEE Trans. Power Electron.*, vol. 29, no. 1, pp. 418–427, Jan. 2014.
[20] S. J. Underwood and I. Husain, "Online parameter estimation and adaptive control of permanent-magnet synchronous machines," *IEEE Trans. Ind. Electron.*, vol. 57, no. 7, pp. 2435–2443, Jul. 2010.
[21] G. Feng, C. Lai, J. Tjong, and N. C. Kar, "Non-invasive Kalman filter based permanent magnet temperature estimation for permanent magnet synchronous machines," *IEEE Trans. Power Electron.*, vol. 33, no. 12, pp. 10673–10682, Dec. 2018.
[22] G. Feng, C. Lai, W. Li, M. Kelly, and N. C. Kar, "Simultaneous stator winding and permanent magnet temperature estimation for permanent magnet synchronous machines," in *Proc. 13th Int. Conf. Elect. Mach.*, Alexandroupoli, Greece, 2018, pp. 1945–1951.
[23] D. Reigosa, D. Fernandez, Z. Zhu, and F. Briz, "PMSM magnetization state estimation based on stator-reflected pm resistance using high-frequency signal injection," *IEEE Trans. Ind. Appl.*, vol. 51, no. 5, pp. 3800–3810, Sep. 2015.
[24] H. Jung, D. Park, H. Kim, S. Sul, and D. J. Berry, "Non-invasive magnet temperature estimation of IPMSM based on high-frequency inductance with a pulsating high-frequency voltage signal injection," *IEEE Trans. Ind. Appl.*, vol. 55, no. 3, pp. 3076–3086, May 2019.
[25] S. Kallio, J. Karttunen, P. Peltoniemi, P. Silventoinen, and O. Pyrhönen, "Online estimation of double-star IPM machine parameters using RLS algorithm," *IEEE Trans. Ind. Electron.*, vol. 61, no. 9, pp. 4519–4530, Sep. 2014.
[26] Z. Li, G. Feng, C. Lai, D. Banerjee, W. Li, and N. C. Kar, "Current injection–based multi-parameters estimation for dual three–phase IPMSM considering VSI nonlinearity," *IEEE Trans. Transport. Electrific.*, vol. 5, no. 2, pp. 405–415, Jun. 2019.
[27] Y. Hu, Z. Q. Zhu, and M. Odavic, "Comparison of two-individual current control and vector space decomposition control for dual three-phase PMSM," *IEEE Trans. Ind. Appl.*, vol. 53, no. 5, pp. 4483–4492, Sep./Oct. 2017.
[28] Z. Li, G. Feng, C. Lai, J. Tian, W. Li, and N. C. Kar, "Dual dc current injection-based stator winding temperature tracking for dual three-phase permanent magnet synchronous machine using Kalman filter," *IET Elect. Power Appl*, vol. 13, no. 11, pp. 1726–1733, Nov. 2019.
[29] J. Karttunen, S. Kallio, P. Peltoniemi, P. Silventoinen, and O. Pyrhönen, "Decoupled vector control scheme for dual three-phase permanent magnet synchronous machines," *IEEE Trans. Ind. Electron.*, vol. 61, no. 5, pp. 2185–2196, May 2014.
[30] S. Kallio, M. Andriollo, A. Tortella, and J. Karttunen, "Decoupled d-q model of double-star interior-permanent-magnet synchronous machines," *IEEE Trans. Ind. Electron.*, vol. 60, no. 6, pp. 2486–2494, Jun. 2013.
[31] Y. Hu, Z. Q. Zhu, and K. Liu, "Current control for dual three-phase permanent magnet synchronous motors accounting for current unbalance and harmonics," *IEEE J. Emerg. Sel. Top. Power Electron.*, vol. 2, no. 2, pp. 272–284, Jun. 2014.
[32] G. Feng, C. Lai, M. Kelly, and N. C. Kar, "Dual three-phase PMSM torque modelling and maximum torque per peak current control through optimized harmonic current injection," *IEEE Trans. Ind. Electron.*, vol. 66, no. 5, pp. 3356–3368, May 2019
[33] M. Thompson, "Practical issues in the use of NdFeB permanent magnets in maglev, motors, bearings, and eddy current brakes," *Proc. IEEE*, vol. 97, no. 11, pp. 1758–1767, Nov. 2009.
[34] S. Li, B. Sarlioglu, S. jurkovic, N. Patel, and P. Savagian, "Comparative analysis of torque compensation control algorithms of interior permanent magnet machines for automotive applications considering the effects of temperature variation," *IEEE Trans. Transport. Electrific.*, vol. 3, no. 3, pp. 668–681, Sep. 2017.
[35] H. W. Kim, M. J. Youn, K. Y. Cho, and H. S. Kim, "Nonlinearity estimation and compensation of PWM VSI for PMSM under resistance and flux linkage uncertainty," *IEEE Trans. Control Syst. Technol.*, vol. 14, no. 4, pp. 589–601, Jul. 2006.
[36] Y. Hu, H. Shoudao, X. Wu, and X. Li, "Control of dual three-phase permanent magnet synchronous machine based on five-leg inverter," *IEEE Trans. Power Electron.*, vol. 34, no. 11, pp. 11071–11079, Nov. 2019.
[37] N. Urasaki, T. Senjyu, and K. Uezato, "Investigation of influences of various losses on electromagnetic torque for surface-mounted permanent magnet synchronous motors," *IEEE Trans. Power Electron.*, vol. 18, no. 1, pp. 131–139, Jan. 2003.
[38] A. H. Abosh, Z. Zhu, and Y. Ren, "Cascaded direct torque control of unbalanced PMSM with low torque and flux ripples," *IEEE Trans. Power Electron.*, vol. 33, no. 2, pp. 1740–1749, Feb. 2018.
[39] K. Liu, Z. Q. Zhu, and D. A. Stone, "Parameter estimation for condition monitoring of PMSM stator winding and rotor permanent magnets," *IEEE Trans. Ind. Electron.*, vol. 60, no. 12, pp. 5902–5913, Dec. 2013.

Guodong Feng (M'15) received the B.S. and Ph.D. degrees in engineering from the Sun Yat-sen University, Guangzhou, China, in 2010 and 2015, respectively.

From 2015 to 2019, he worked as a Postdoctoral Fellow with the University of Windsor, ON, Canada. He is currently an Associate Professor with the School of Intelligent Systems Engineering, Sun Yat-sen University, China. His research interests include advanced signal processing, optimization, and electrical machines and drives.

Chunyan Lai (SM'19) received the B.S. degree in engineering from Sun Yat-sen University, Guangzhou, China, in 2010, the Ph.D. degree in ECE from the University of Windsor, Windsor, ON, Canada, in 2017.

From 2017 to 2018, she was a Postdoctoral Fellow with the University of Windsor, Windsor, ON, Canada. She is currently an Assistant Professor with the Department of Electrical and Computer Engineering, Concordia University, Montreal, QC, Canada. Her research interests include electric machine drives and controls and other power electronics related applications such as renewable energy.

Wenlong Li (SM'15) received the B. Eng degree from Sichuan University, Chengdu, China, in 2005, the M. Eng degree from the University of Science and Technology of China, Hefei, China, in 2008, and the Ph.D. degree from the University of Hong Kong, Hong Kong, in 2012.

He is currently a Visiting Scholar with the University of Windsor, Windsor, ON, Canada. He has authored and coauthored over 70 peer-viewed technical papers and three invited book chapters in these areas. His research interests include electrical machine design, analysis, and applications.

Ze Li (GSM'17) received the B.Eng and M.Eng degrees from the Xi'an University of Architecture and Technology, Xi'an, China in 2012 and 2015 respectively. He is currently working toward the Ph.D. degree with the University of Windsor, Windsor, ON, Canada.

In 2017, he worked as a Testing Engineer with D&V electronics Co., Ltd, Woodbridge, ON, Canada. His research interests include modeling and control of electric power converters and electrical machines, and machine parameter identification, testing, and performance analysis.

Narayan C. Kar (SM'07) received the B.S. degree in electrical engineering from the Bangladesh University of Engineering and Technology, Dhaka, Bangladesh, in 1992, and the M.S. and Ph.D. degrees in electrical engineering from the Kitami Institute of Technology, Hokkaido, Japan, in 1997 and 2000, respectively.

He is currently a Professor with the Department of Electrical and Computer Engineering, University of Windsor, ON, Canada, where he also holds the Canada Research Chair position. His research interests include analysis, design, and control of electrical machines for electrified vehicle applications.